THE JOURNAL OF PHYSICAL CHEMISTRY C
A JOURNAL OF THE AMERICAN CHEMICAL SOCIETY

pubs.acs.org/JPCC

Article

A Microscopic View of Macromolecule Transfer in the Vacuum Using Gas and Bismuth Clusters

Arnaud Delcorte*

Cite This: J. Phys. Chem. C 2022, 126, 7307−7318

Read Online

ACCESS | Metrics & More | Article Recommendations | Supporting Information

ABSTRACT: Transferring large nonvolatile molecules in the vacuum is key to both their characterization by mass spectrometry (ion mobility, etc.) and their use as nanofabrication building blocks in soft-landing-type experiments. Recently, our group performed the successful transfer and redeposition of intact and bioactive lysozyme (14 kDa) with large gas cluster ion beams, in the absence of a solvent or matrix, demonstrating that such beams could serve as tools for macromolecule manipulation. A number of fundamental questions arose in relation with this experimental proof-of-concept, concerning for instance the maximum molecular size for successful transfer, the effect of the cluster projectile incidence angle, the dependence of molecular dissociation on the projectile energy and size, the internal energy uptake ultimately leading to metastable decay reactions, or the influence of the surface interactions on desorption. To address these questions, a series of molecular dynamics simulations were conducted involving cluster impacts on an adsorbed globular polystyrene (PS) macromolecule of 60 kDa, with a mass and shape comparable to those of a protein such as bovine serum albumin. Conditions of intact desorption of this PS molecule by Ar clusters are identified, in terms of energy per atom and incidence angle, and the results are compared to 30 keV Bi_5 impacts, commonly used for molecular analysis and 2D imaging in our time-of-flight secondary ion mass spectrometry experiments. When Ar cluster impact conditions are appropriate for intact desorption, the take-off angle of the macromolecule is larger than the projectile incidence. Bombardment by a massive methane projectile (6.6×10^4 methane molecules) does not induce qualitatively different results, and in general, the energy per atom or energy per unit mass remains the deciding factor concerning the survival or dissociation of the bombarded molecule. In contrast with large gas clusters, Bi_5 projectiles largely fail at desorbing the intact macromolecules, because of the detrimental effect of the collision cascade and the insufficient momentum transferred by the crater expansion for molecular lift off. Additionally, 10 keV Ar_{5000} projectiles with 45−75° incidence with respect to the surface normal directly transfer momentum to the macromolecule via their backscattered Ar atoms and small clusters, inducing molecular desorption with center-of-mass velocities of the order of 1 km/s. The implications for future experiments are discussed.

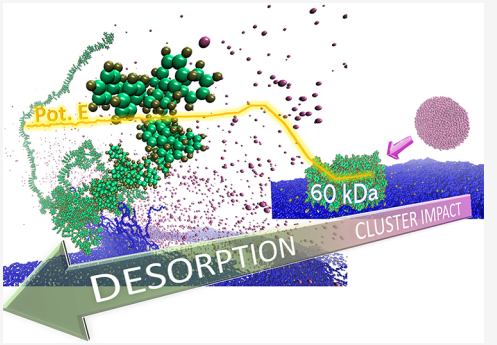

1. INTRODUCTION

The ability to manipulate large nonvolatile (bio)molecules to either analyze them or to design new organic and hybrid architectures at the nanoscale represents an important scientific and technological achievement. In general, the methods for identifying nonvolatile (bio)molecules and for arranging them in thin layers, arrays, or patterns rely on the use of liquid and sometimes solid solutions. Adsorption from aqueous solution is the most widespread approach for protein film formation,[1] though it may exhibit some shortcomings such as activity loss due to conformational changes,[2] poor control of the deposited quantity, and limitation to one monolayer.[3] Alternatively, soft landing uses (preparative) mass spectrometry (ESI, MALDI) to deposit large biomolecules on surfaces, which also involves dissolution of the molecules in an aqueous solvent or an acidic matrix.[4] The molecular ions are then transferred into the gas phase and landed onto a designated substrate, with the possibility of patterning by motion of the collector or ion deflection prior to landing. The same ionization and ion selection techniques are also used to mass analyze similar molecules in tissues and even single cells.[5] In all the (nano)fabrication methods involving biomolecules such as proteins, the issue of preserving the molecular conformation is central, since it governs bioactivity.

Recently, our team has shown that proteins like lysozyme could be transferred intact onto a collector following their desorption from a solid target reservoir using large cluster ions ($Ar_{3000-5000}^+$) accelerated to a kinetic energy of 5−10 keV.[6] Moreover, bioassays conducted on the collected material demonstrated that a large fraction of the transferred enzymes

Received: February 18, 2022
Revised: April 4, 2022
Published: April 15, 2022

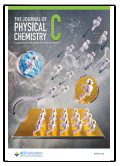

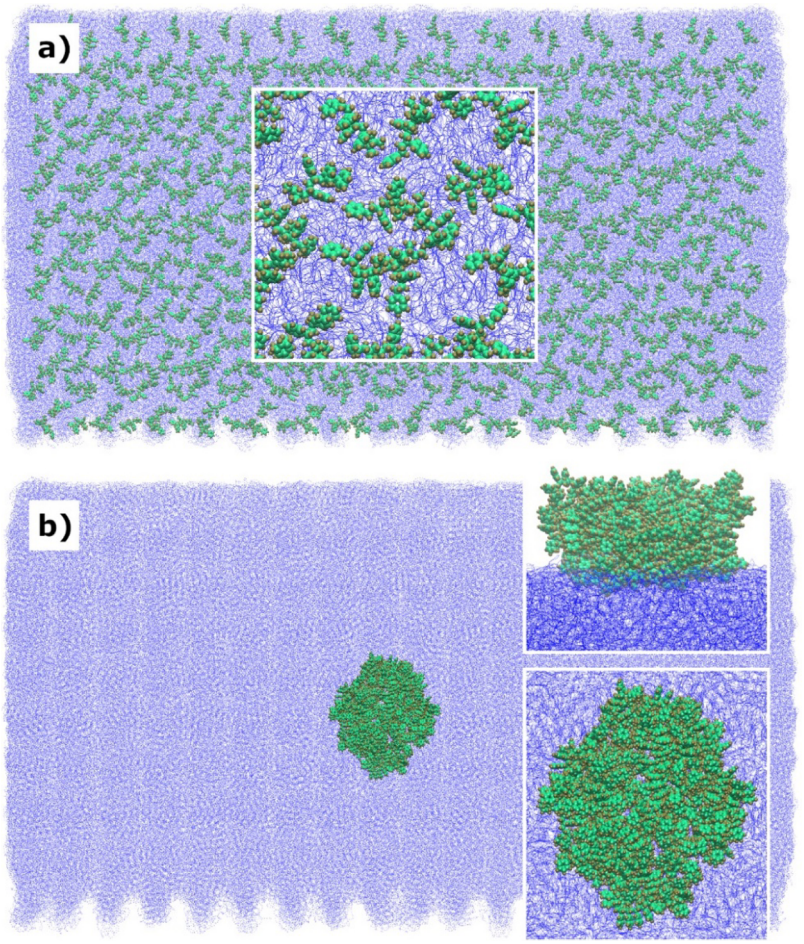

Figure 1. Surface configuration of the organic samples. Panels (a,b) show top views of samples 1 and 2. The carbon and hydrogen atoms of the atomistic PS molecules are represented by light green and tan colors, respectively. The coarse-grained PE chains are represented by blue lines. The inset of panel (a) shows a zoom of the central part of sample 1. The insets of panel (b) display close-up side (above) and top (below) views of the PS500 molecule of sample 2.

remained bioactive. In contrast with other methods, the argon cluster ion beam transfer or iBEAM method uses pure solid samples devoid of solvent or matrix molecules and is not restricted to molecular ions since the material is transferred irrespective of its charge state. One drawback is that direct patterning with the beam is impossible (the deposition pattern mirrors the angular distribution of sputtered molecules), but on the other hand, much larger fluxes can be attained than by selecting only charged molecules. Beside lysozyme, a range of MALDI matrices[7,8] and kilodalton molecules including polystyrene oligomers, Irganox 1010, angiotensin, and insulin could also be transferred undamaged.[9−11] The fraction of intact molecules was inversely proportional to the energy per atom (E/n) of the impinging cluster ions. Though this variant of soft landing appears to be a promising new technique for building up complex molecular or hybrid multilayers on virtually any substrate material, a number of fundamental questions still remain open. For instance, (i) what is the maximum molecular size that can be desorbed and how does it depend on the cluster size? (ii) How are the internal energy and the conformation of the molecules influenced by the desorption conditions (cluster size, energy, incidence angle, etc.[12])? (iii) Would much larger clusters or clusters with a different chemistry be more appropriate to transfer "cool" molecules (thereby preserving their initial conformation)? These questions, applied to molecular ions, are also at the core of cluster-induced secondary ion mass spectrometry (SIMS) of large (bio)molecules, a label-free imaging method that enables 3D molecular localization in solid organic and biological samples with an unprecedented lateral and depth resolution.[13−17]

To explore the fundamental issues, theoretical investigations based on molecular dynamics (MD) computer simulations constitute a method of choice because they offer mechanistic insights that are out of reach of experiments.[18] They have long been used to study atom and cluster bombardment of inorganic and organic surfaces, starting with the pioneering works of Harrison et al.[19] and Garrison.[20] There also exist a number of reports on large cluster bombardment of surfaces,[21−26] including Ar cluster bombardment of organic[27] or even biological molecular solids.[28] The cratering, emission, and molecular fragmentation processes,[29] as well as the dependences on the incident ion parameters (E, n, and incidence angle[30]), have been largely explained. Alternatively, MD studies have been devoted to studying the interaction of low energy molecules with surfaces in order to elucidate soft- and reactive-landing mechanisms.[31,32] However, to our knowledge, there does not exist an atomistic MD study so far devoted to the gas cluster ion-induced emission of macromolecules of a size comparable to that of proteins (>50 kDa), which is also pushing the currently admitted experimental limits of SIMS.

https://doi.org/10.1021/acs.jpcc.2c01196
J. Phys. Chem. C 2022, 126, 7307−7318

In this article, MD simulations are used to investigate the aforementioned questions. First, the dependence of medium-size molecule (0.6 kDa) emission on the incidence angle of 10 keV Ar_{5000} projectiles is computed, showing a maximum yield between 40 and 60° with respect to the surface normal. Then, the effects of large Ar cluster impacts on the displacement and desorption of a 60 kDa macromolecule are studied and compared to the case of small bismuth cluster impacts (bismuth cluster sources have become the standard in SIMS imaging because they ensure optimum lateral resolution together with high ion yields). The comparatively better efficiency of large Ar clusters for desorbing large molecules is explained mechanistically. The influence of the Ar cluster incidence angle on desorption is also elucidated. As a perspective, large molecule desorption by 5−10 keV Ar_{5000} (200 kDa) is compared to desorption by a much larger organic nanodrop, namely, $(CH_4)_{66396}$ (1.6 MDa).

2. COMPUTER SIMULATIONS

The molecular dynamics simulation program used in this study was the SPUT code developed by the group of B. J. Garrison at Penn State University for sputtering applications.[18] In the classical MD method, Hamilton's equations of motion are numerically integrated over a given time interval, providing us with the position and velocity of each particle at each timestep. Forces among the atoms or particles in the system are derived from empirical interaction potentials.

In order to limit the computational expense, the two purely organic samples used for this study were hybrid, using a coarse-grained substrate and carrying hydrocarbon molecules described at the atomistic level (Figure 1a,b). The first sample (sample 1) consists of a monolayer of small polystyrene tetramer molecules (PS4: 0.55 kDa), while the second (sample 2) is a large polystyrene molecule with 500 repeat units (PS500: 60 kDa), both relaxed on the same coarse-grained substrate. The polyethylene (PE) substrate and the methodology of coarse graining have been described in detail in previous articles.[33,34] It was made of a collection of 8100 chains of 97 CH_2 united atoms (14 amu) capped with 2 CH_3 united atoms (15 amu), for a total system size of 50.3 nm × 29.2 nm × 18.8 nm. The interaction potentials were Lennard-Jones potential functions for intermolecular (nonbonding) interactions and Morse potential functions for the intramolecular (covalent) interactions in the chains.[35] For the most realistic description of the atomistic C−C and C−H interactions, the AIREBO potential was chosen, enabling bond scissions and formation and including long-range interactions.[36] Hydrogen (^1H) was replaced with tritium (^3H) for computational efficiency. The nonbonding interactions between C and H atoms and coarse-grained units were taken from previous investigations.[23] All the simulations were conducted using a damping zone at the bottom and on the four lateral sides of the PE substrate (Langevin algorithm with a friction coefficient) in order to absorb the pressure waves and mimic a semi-infinite, bulk sample.[37] A series of calculations involving large clusters and the PS500 molecule was also conducted using thin gold substrates (sample 3). The Au(111) surfaces were monocrystals with either 3 or 6 atomic layers, with a bottom layer held rigid and the others being stochastic (Langevin algorithm). The Au−Au interactions were modeled using the molecular dynamics/Monte Carlo corrected effective medium (MD/MC-CEM) many-body potential.[38] The Au−C and Au−H interactions were Lennard-Jones potential functions with the parameters given in ref 39. At variance with small cluster impacts, comparisons with a single layer held rigid[40] (similar to a repulsive wall[41,42]) showed no significant difference concerning the dynamics of massive cluster shattering and molecular emission. With the potentials described above, the binding energy of the PS500 molecule on the PE substrate was 56 eV (0.11 eV/PS monomer) and on the gold substrate was 26 eV (0.05 eV/PS monomer).

Ar_{5000} clusters were modeled using Lennard-Jones potentials splined to the KrC repulsive potential at a short interdistance.[43] A purely repulsive Molière potential was used to describe the Ar interactions with other atoms in the solid. The methane cluster $(CH_4)_{66396}$ was described using the AIREBO potential (see supra). A 6−12 Lennard-Jones potential function was used for the description of the Bi−Bi interaction in the Bi_5 clusters, as was the case in a previous study.[44] The equilibrium distance and energy well depth were taken from first-principles for Bi neutral clusters.[45] Accordingly, the Bi_5 cluster geometry was chosen as a pyramid. Lennard-Jones potential functions splined to a Molière function at a small interdistance were used to describe the repulsive wall and the nonbonding interactions of Bi with the sample atoms. Because prior sputtering simulations showed no significant variation related to the Bi_5 cluster orientation toward the organic target,[44] only one orientation was selected here.

3. RESULTS AND DISCUSSION

3.1. Molecular Emission upon Ar Cluster Bombardment. Before investigating the cluster bombardment of a large globular PS molecule made of 500 repeat units (Figure 1b), the molecular emission dependence on the cluster incidence angle was computed for an overlayer of small PS oligomers on the soft PE substrate (Figure 1a). Routine SIMS analysis[46] and molecular transfer under the vacuum using Ar_{5000}^+ projectiles (Figure S-1) demonstrate that small PS oligomers can be desorbed, ionized, and collected without damage in experiments. Figure 2 shows the sputtered mass as a function of the incidence angle with respect to the surface normal of PS tetramers (full circles) and of all emitted species including the PE substrate (open diamonds). Each data point is the average of two bombardments with different aiming points on the surface.

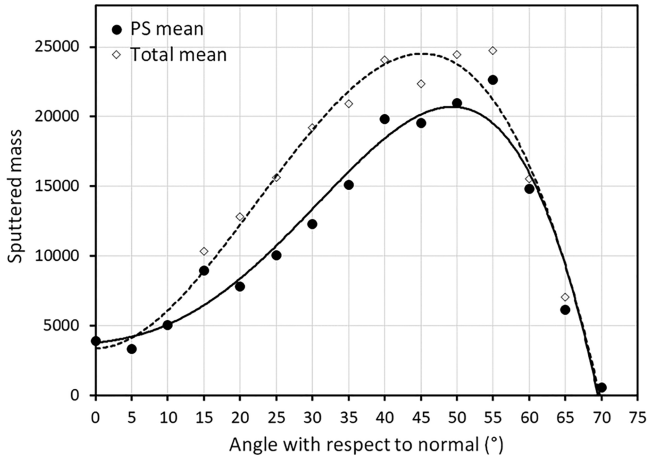

Figure 2. Ar_{5000} (10 keV) bombardment of sample 1. Dependence of the sputtered mass on the incidence angle of the projectile (with respect to the surface normal). Each point is the average of two impacts. Black dots: surface PS molecules; open diamonds: total sputtered mass (including substrate PE chains).

https://doi.org/10.1021/acs.jpcc.2c01196
J. Phys. Chem. C 2022, 126, 7307−7318

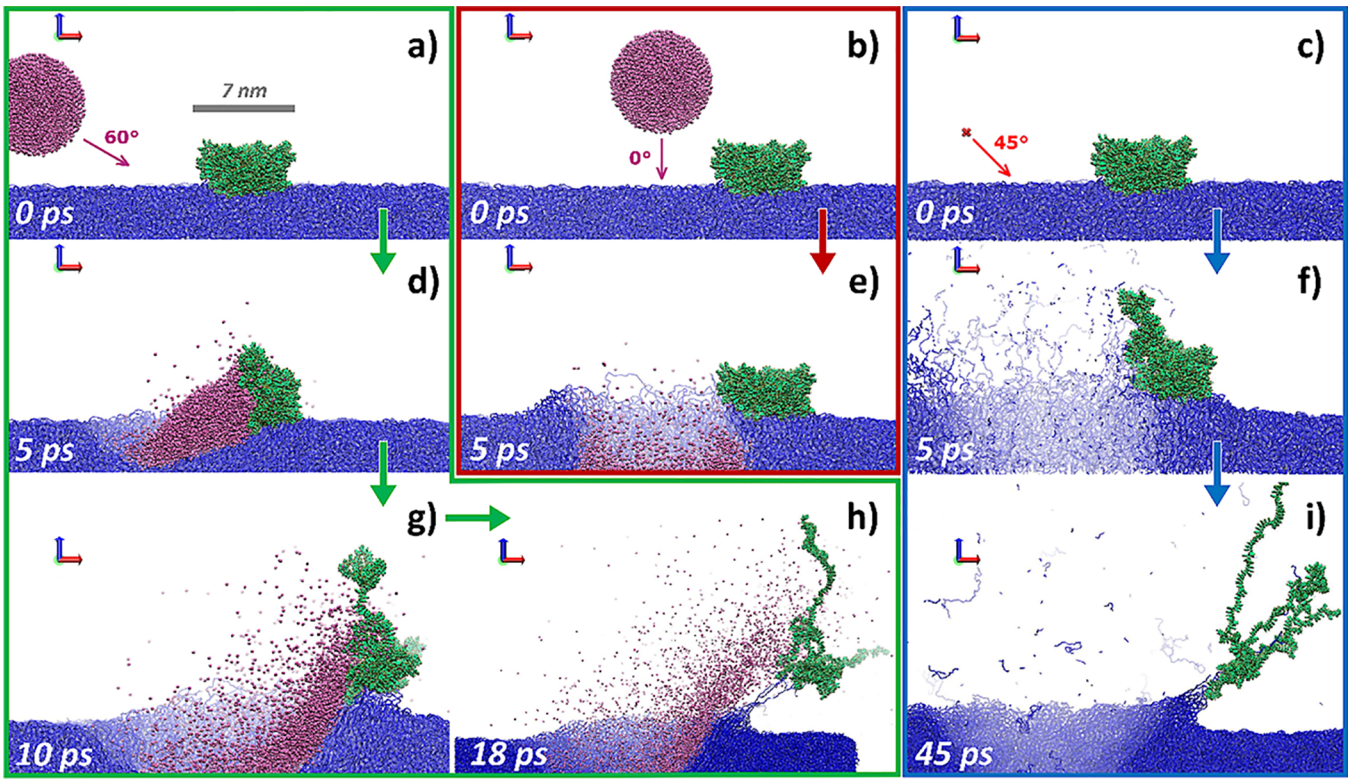

Figure 3. Time evolution of three characteristic trajectories involving sample 2. (a,d,g,h; green frame) 10 keV Ar_{5000} impact with 60° incidence on the side of the PS500 molecule: (a) 0 fs, (d) 5 ps, (g) 10 ps, and (h) 18 ps. (b,e; red frame) 10 keV Ar_{5000} impact with 0° incidence on the side of the PS500 molecule: (b) 0 fs and (e) 5 ps. (c,f,i; blue frame) 30 keV Bi_5 impact with 45° incidence on the side of the PS500 molecule, see aiming point A in Figure 4; (c) 0 fs, (f) 5 ps, and (i) 45 ps. The incident Ar atoms are represented by pink spheres. For the other atoms, the color coding is the same as Figure 1. Thick green, red, and blue arrows indicate the order of the snapshots for each MD trajectory.

The maximum number of ejected PS molecules in one impact is 41, and it is observed at 55° incidence.

Although the sample and the projectile were different, the observed angular dependence is reminiscent of the one calculated by Czerwinski et al. for coarse-grained benzene bombarded by 14.75 keV Ar_{2953}.[30] It shows the characteristic maximum around 45−50° and the rapid decrease beyond 60°. The difference between the value at 0° and at the maximum is a factor of ∼5 in our case, which is more than their calculations. The literature also gives us access to the experimental angular dependence of the sputtering yield for solid Irganox 1010 samples bombarded by large Ar clusters.[47] For 10 keV Ar_{5000} bombardment (E/n = 2 eV), Seah et al. report a maximum emission at 45° and a factor >5 difference between the sputtering yield at 45 and 0° incidence. The same article shows that this factor decreases with increasing E/n, which is also consistent with the calculations of ref 30., where E/n = 5 eV. The reasons of the lower emission observed at normal versus 45° incidence were explored in refs 27 and 30 and involve blocking of the surface molecule ejection by the projectile atoms and energy deposition deeper in the soft organic matter, which both hamper sputtering.

A few additional points should be noted. First, sample 1, where the top layer (PS tetramers) is different compared to the substrate (coarse-grained PE, $C_{99}H_{200}$), indicates that, for Ar_{5000} bombardment, most of the emission comes from the PS overlayer and that the maximum emission from the underlying PE is at a lower angle (between 25 and 35°), which can be explained by the dynamics of the crater formation. Second, the radial expansion of the crater causes the PS molecules to accumulate at the crater outskirt during the emission process, so that dimers and sometimes larger multimers are identified in the sputtered flux even though the molecules were not linked on the initial surface (Figure S-2). Finally, our results indicate that the emission drops to zero with an incidence angle of 70°, at slight variance with the reported experiments where some emission is still observed for larger angles.[47] Two effects might contribute here: first, the nanoscale roughness of the samples in the experiments, leading to slightly different incidence angles upon impact, and second, the size distribution of the real Ar clusters around the nominal value.

For the study of emission of a PS500 macromolecule induced by 10 keV Ar_{5000} impacts (sample 2), a decision had to be made concerning the impact points to be probed since the computations can be quite time-consuming. Based on previous studies involving smaller molecules, which showed that direct hits at the molecules or impacts too far away from them did not lead to emission,[29] we selected an impact point on the side of the molecule, at a distance of ∼3.5 nm of its edge, which roughly corresponds to the radius of the cluster (Figure 3a,b). Since the molecule is globular, this aiming point is representative of any other point located at a similar distance around the molecule. It should be optimal for molecular emission. Nevertheless, two other aiming points were tested with a 45° polar incidence angle, for an x position moved by 3.5 nm on each side of the aforementioned one, i.e., one aiming point directly on the molecule and one 7 nm away from it. The direct impact buries the molecule in the crater, while the one at 7 nm causes molecule displacement and elongation along the cluster incidence direction but no emission.

https://doi.org/10.1021/acs.jpcc.2c01196
J. Phys. Chem. C 2022, 126, 7307−7318

Table 1. Quantitative Indicators for a Series of Impact Events Involving the PS500 Macromolecule

cluster	energy (keV)	E/n (eV/cc)	angle (°)	desorption	molecule velocity (km/s)	molecule direction (°)
			polyethylene substrate			
Ar_{5000}	10	2	0	no	0.03[a]	33.9[a]
Ar_{5000}	10	2	15	no	0.15	115.1
Ar_{5000}	10	2	30	no	0.28	91.0
Ar_{5000}	10	2	45	yes	1.04	59.6
Ar_{5000}	10	2	60	yes	1.67	68.3
Ar_{5000}	10	2	75	yes	1.51	81.8
Bi_5 (A)[b]	30	6000	45	no	0.18	95.3
Bi_5 (B)[b]	30	6000	45	yes	0.40	45.5
			gold substrate			
Ar_{5000}	10	2	45	yes	2.13	82.2
Ar_{5000}	20	4	45	yes	3.14	80.6
Ar_{1000}	10	10	45	yes/F[c]	2.51	75.4
$(CH_4)_{66396}$	20	0.3	45	yes	1.35	83.5
$(CH_4)_{66396}$	66	1	45	yes	2.78	80.6
$(CH_4)_{66396}$	200	3	45	yes	4.90	80.2
$(CH_4)_{66396}$	664	10	45	yes/F[c]	8.92	79.0

[a]Value at 10 ps, when the trajectory was terminated. [b]Letters "A" and "B" refer to specific aiming points described in Figure 4. [c]Letter "F" signifies that the molecule was fragmented upon emission.

For the first aiming point, at 3.5 nm of the PS500 molecule edge, the polar incidence angle was varied between 0° (normal to the surface) and 75° by steps of 15°. The main results of these simulations are reported in Table 1, and the examples of the dynamics are provided in Figure 3, for 0 and 60° impacts. The results indicate that there is a range of incidence angles for which desorption is favored, from >30 to 75°. As shown in Figure 3b,e (red frame), normal impacts form a deep crater beside the molecule and only lead to a minor vertical displacement of the organic matter at the rim, before dissipation of the energy and stabilization of the PS500 molecule. In contrast, a scenario of the successful desorption of the PS500 molecule is shown in Figure 3a,d,g,h (green frame), which corresponds to an incidence angle of 60°. In that case, in addition to the crater and rim formation gently lifting the molecule after a few picoseconds, there is the additional effect of the initial cluster momentum along the x direction (horizontal), which pushes the molecule sideways either directly or after partial backscattering from the forming crater slope (Figure 3d). These combined effects suffice to disentangle the molecule from the sticking substrate PE chains (Figure 3h) and finally eject it with a significant vertical velocity component.

For all the considered angles, Table 1 reports the center-of-mass velocity and the take-off angle of the macromolecule when it is desorbed or at a time when its fate is certain (between 10 and 80 ps depending on the incidence). Impacts between 45 and 75° constitute clear-cut intact molecular desorption cases but with a take-off angle always larger than the incidence angle and increasing proportionally. Therefore, the 75° impact, with a molecular take-off angle of 82°, seems to be at the limit of possible emission in the case of a real system where a number of molecules would be present on the surface or where the surface would have a somewhat larger natural roughness. For the considered impacts, the center-of-mass velocity of the molecule is rather high at the end of the trajectory (above 1 km/s), mirroring the significant momentum transfer from the projectile. The impact with an incidence of 30° constitutes an interesting limit case (Figure S-3). Indeed, the macromolecule lifts up with a significant momentum while gradually unfolding as it moves upward. However, beyond 50 ps, it is completely extended in the vacuum and yet attached to the surface via nonbonding interactions with a number of polyethylene chains. Eventually, the center-of-mass velocity vector angle with the normal exceeds 90°, indicating that the molecule tends to fall back toward the surface and will not have sufficient momentum to severe its bonds and escape.

3.2. Comparison with Bi_5 Clusters. It has been argued in the literature and there seem to be some experimental indications that large clusters such as Ar_{5000}^+ are more efficient to emit large molecules compared to smaller clusters used in SIMS, typically Bi_n^+ or C_{60}^+.[10] However, because the SIMS technique detects only ions, the two effects of sputtering and ionization remain entangled in the observations. On the one hand, comparisons of ion yields inevitably involve ionization probabilities and the underlying ion formation mechanisms, which might vastly vary when comparing small and large clusters (and so might their energy dependences). On the other hand, sputter yield measurements based on crater size in the target or mass of the redeposited material on a collector consider all the sputtered species, including entire molecules as well as their fragments, so they fail at informing us on the relative quantities of molecules sputtered intact.

Here, sample 2 was selected to test the possibility of large molecule emission by small Bi clusters. Bi_5 clusters (30 keV) were chosen as projectiles because these nuclearity and energy are routinely used in our SIMS analysis and imaging experiments. Note that their kinetic energy is 3 times larger than that used for the Ar_{5000} impacts, which should result in larger scale craters and collective motions in the organic solid. The chosen incidence angle (45°) is also the most common one in the existing experimental setups. Only one orientation of the pyramidal cluster was considered for reasons explained in the methodological section. With all these parameters set, a point of special care concerned the choice of the aiming points on the surface. In order to test a number of configurations yet keeping the computational expense reasonable, 17 aiming points were tested, as indicated by red diamonds in Figure 4.

In Figure 4, all the impact points, which are not associated to a blue circle, correspond to trajectories where the PS500 molecule (in green) is ultimately damaged, i.e., covalent bonds get broken.

https://doi.org/10.1021/acs.jpcc.2c01196
J. Phys. Chem. C 2022, 126, 7307−7318

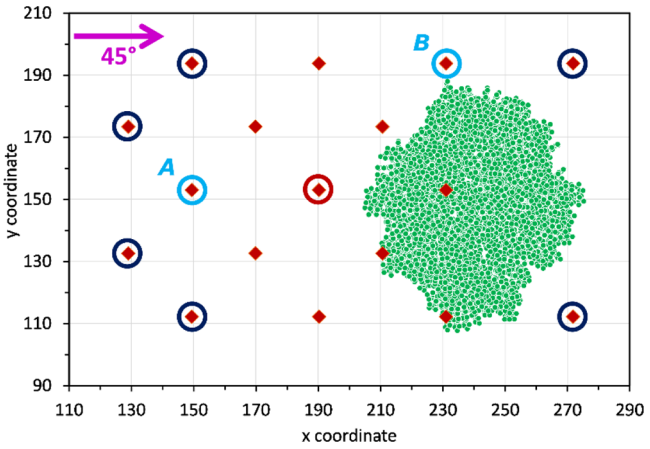

Figure 4. *x* and *y* coordinates (in Å) of the aiming points on the target (red diamonds) for 30 keV Bi_5 bombardment of sample 2. No circle or a red circle signifies that the PS500 molecule is fragmented by the interaction (see Figure 5), dark blue circles indicate neither significant uplifting nor fragmentation of the PS500 molecule, and light blue circles correspond to cases where the molecule completely unfolds above the surface without dissociating (see Figure 6).

A few of the aiming points lead to direct hits at the macromolecule, which obviously result in its extensive fragmentation. At variance with Ar_{5000} bombardment, a large number of impacts in the substrate also lead to the PS molecule fragmentation via energetic recoil atoms from the collision cascade. One such trajectory, corresponding to the impact point with the red circle in Figure 4, is illustrated in Figure 5. Figure 5a,b shows side views of the dissociated PS molecule on its way to the vacuum after 6 ps, with the link between the different fragments indicated by thin green lines in (b). The time evolution of the collision cascade is shown in Figure 5c by the successive positions of the energetic atoms integrated over the first 500 fs of the interaction. It suggests that a few recoil atoms from the substrate penetrate the PS molecule where they eventually severe some C−C and C−H bonds. Figure 5d shows a close-up perspective view of such a recoil atom traveling through the PS macromolecule. In this case and a number of others, the close inspection of the collision cascade development in the very early part of the interaction suffices to demonstrate the fragmentation of the PS500 molecule. In a few other cases, the MD simulation had to be run for longer times to observe fragmentation. The impact and energy deposition behaviors, involving recoil atom cascades for Bi_5 and purely collective effects for Ar_{5000}, are a direct consequence of the vastly different kinetic energies of the projectile atoms, 6000 eV for each Bi against 2 eV for each Ar constituent atom.

For some trajectories, the energy deposition via the collision cascades, which form around the tracks of the projectile atoms propagating inside the PE substrate with an angle close to the initial 45° (as seen in Figure 5c), is simply too far away from the molecule to induce desorption (dark blue circles in Figure 4). The two remaining impact points (light blue circles) constitute limit cases where the PS molecule remains intact and receives a significant amount of upward momentum that could possibly lead to desorption. The case of impact A is similar to the 30° Ar_{5000} impact trajectory, where the molecule tends to expand in the vacuum while being still attached to the surface at one end (van der Waals interactions with the substrate PE chains, Figure 3i). As a result, the angle made by the center-of-mass velocity vector with the surface normal keeps increasing with time, until it becomes too large for emission (>90°). The situation of impact B, however, finally leads to molecular emission together with some attached PE oligomers beyond 75 ps (Figure 6). In that case, the upward moving polymer chains (PS500 and PE) slide along the ones that remain attached to the surface, until they free themselves from the surface with still significant upward momentum. The desorbing macromolecule is in a fully extended conformation.

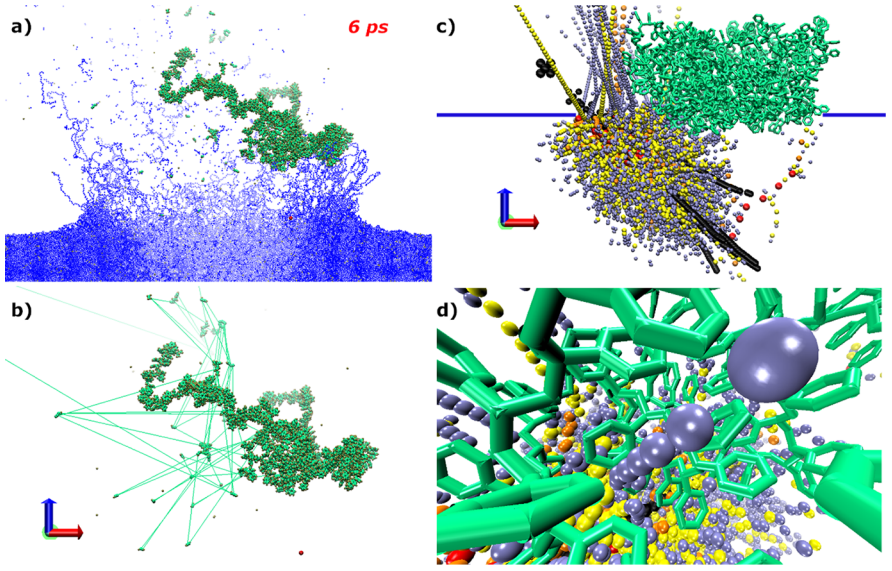

Figure 5. Analysis of a trajectory (aiming point with a red circle in Figure 4) where the interaction with the Bi_5 projectile leads to the PS500 molecule fragmentation (sample 2). (a,b) Side views of the situation at 6 ps, represented with (a) or without (b) the PE substrate. In panel (b), the thin green lines signify C−C and C−H bonds severed by the interaction. (c) Representation of the collision cascade over the first 500 fs of the interaction. The successive positions of the recoil atoms are indicated by colored spheres (every 250 timesteps), provided that they are set in motion with more than 15 eV of kinetic energy. Black spheres: Bi_5 projectile; other colored spheres: red ≥ 300 eV ≥ orange ≥ 100 eV ≥ yellow ≥ 30 eV ≥ blue ≥ 15 eV of kinetic energy. (d) Perspective view of a detail of panel (c), showing a recoil atom traveling inside the PS500 molecule.

https://doi.org/10.1021/acs.jpcc.2c01196
J. Phys. Chem. C 2022, 126, 7307−7318

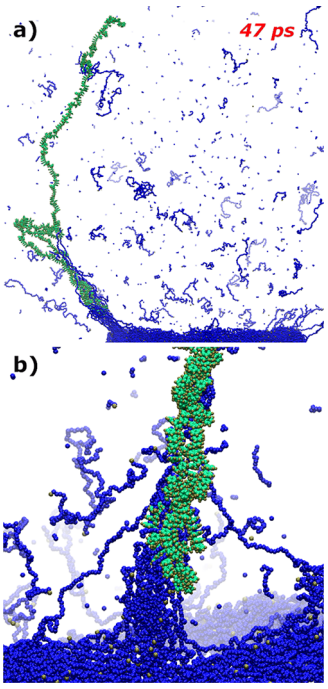

Figure 6. Snapshots of a trajectory (aiming point B with a light blue circle in Figure 4) where the interaction induced by the Bi_5 projectile leads to the PS500 molecule unfolding in the vacuum (sample 2). (a) Side view of the crater rim and ejecting species at 47 ps; (b) close up view of the link between the PE substrate chains and the departing PS500 molecule. The view is rotated horizontally by ∼90° counterclockwise with respect to panel (a).

As was observed in other studies, both energetic large (Ar_{5000}) and small (Bi_5) clusters create nanoscale craters in the organic substrate within a few picoseconds, inducing large scale collective motions that are key to sizeable molecule emission. In the first case, the pressure waves and collective motions are immediately induced by the interaction of the projectile as a whole with the solid. In the second case, the cluster constituents penetrate ∼10 nm in the solid surface, generating overlapping atomic cascades, which eventually induce outward pressure waves and molecular motions upon cooling.

3.3. Effect of the Substrate. A series of simulations of Ar_{5000} impacts was computed with a third sample where the PS molecule was adsorbed on gold (111) (sample 3, Figure S-4). In general, for cluster energies lower than ∼10 eV/atom and aiming points close or even involving the PS macromolecule, intact desorption is observed. An example is given in Figure 7a−c for a 45° impact trajectory where the cluster hits both the substrate and the molecule. Again, the cluster transfers part of its momentum along the x direction to the molecule, which slides sideways. In this case, both the reaction of the molecule after its vertical compression by the impinging cluster and the vertical momentum transferred by a fraction of the backscattered Ar atoms provide the necessary upward velocity component. Even impacts with 0° incidence on the side of the molecule lead to its ejection. When the impact zone does not encompass the molecule, only the backscattered Ar atoms provide momentum to the molecule via a so-called washing mechanism. This mechanism explains the usefulness of large noble gas clusters for surface cleaning of inorganic surfaces such as silicon oxide in the microelectronics industry. In all these simulations, the molecule departs the surface with a take-off angle close to 80° (Table 1),

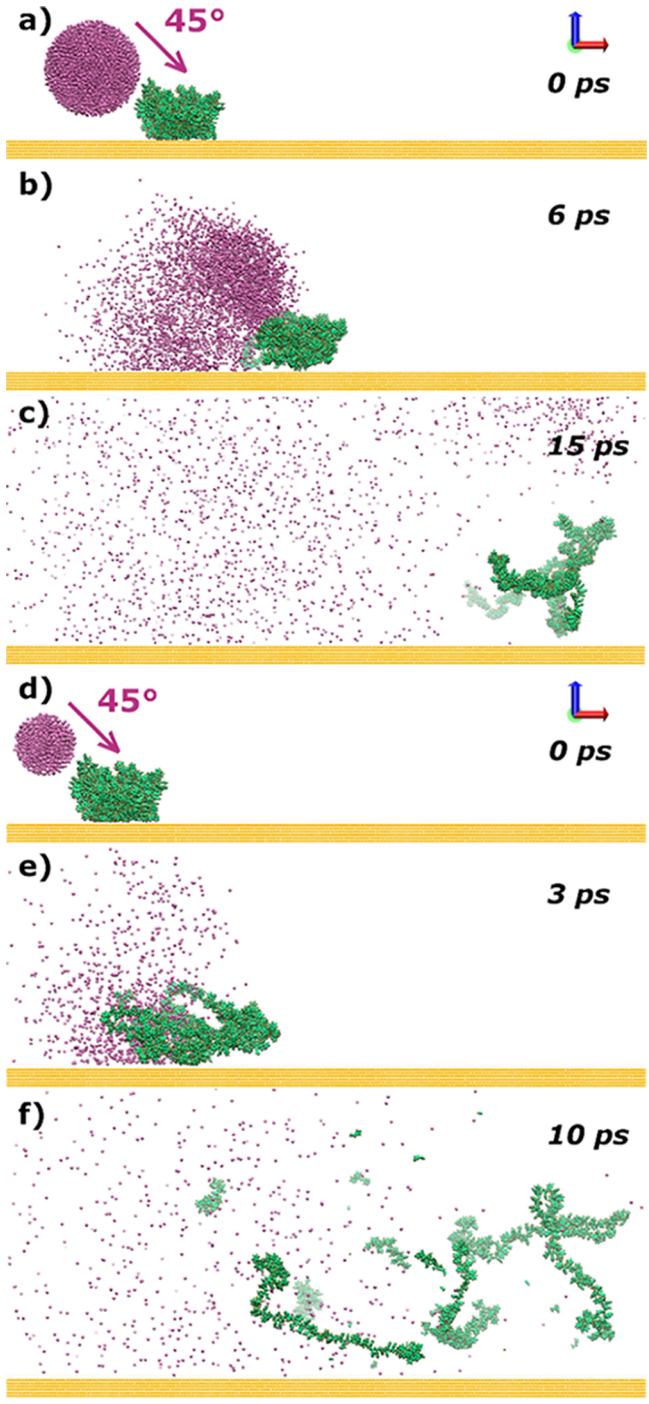

Figure 7. Time evolution of two trajectories involving sample 3. (a−c) Ar_{5000} (10 keV) impact (45° incidence) on the side of the PS500 molecule adsorbed on Au(111): (a) 0 ps, (b) 6 ps, and (c) 15 ps. (d−f) Ar_{1000} (10 keV) impact (45° incidence) on the side of the PS500 molecule: (d) 0 ps, (e) 3 ps, and (f) 10 ps.

which is also made possible by the atomically flat Au crystal surface used as a substrate. The results might be slightly different with a more realistic and corrugated substrate. In comparison with the organic PE substrate, the ejecting molecules are also 2−3 times faster, which translates in considerably larger center-of-mass kinetic energies. When the cluster E/n increases to 10 eV, the emission process does not change significantly but the Ar atoms now have sufficient kinetic energy to induce bond scissions upon collision with the C and H atoms of the PS

https://doi.org/10.1021/acs.jpcc.2c01196
J. Phys. Chem. C 2022, 126, 7307−7318

molecule. The process is illustrated in Figure 7d−f with a 10 keV Ar_{1000} cluster impact. Though it is not the only factor, the fact that the binding energy of the PS500 molecule to the gold is about half that with the PE substrate (26 eV versus 56 eV) should also favor desorption.

In these simulations, only six large gold layers (3×10^5 Au atoms in total) were computed to describe the substrate behavior, and similar results were obtained using a single rigid layer (repulsive wall), as did some other authors, too.[41,42] Testing substrates with six gold layers allowed us to demonstrate that the heavy metal substrate is essentially unaffected (very few displaced atoms) and reacts almost elastically for $E/n \leq 5$ eV, as would a purely repulsive wall. It is possible that pressure waves generated in the gold crystal are not fully damped as they would with a thicker monocrystal[22,48] and that some spurious energy reflection to the surface occurs. However, at low energy per atom (0−3 eV), oblique incidence (45°), and for such a carbon-based molecule adsorbed on a heavy gold substrate, this effect should have a negligible incidence on the results. This is supported by the consistency of our new simulations with the earlier ones involving smaller molecules and a thicker Au substrate.[48]

3.4. Massive Cluster Projectiles. The following question arises from the use of increasingly large clusters for molecular desorption: is there proportionality between the size of the cluster and the maximum molecular size that can be desorbed intact? Or could even larger clusters enable reaching smaller projectile E/n providing (i) still intact macromolecule desorption and (ii) lower internal energies so that the macromolecule should survive for longer times after emission and keep a conformation closer to the original one? A thorough exploration of these questions is beyond the scope of this article. However, inspired by some experimental studies,[49,50] we carried out a series of MD simulations involving methane (CH_4) molecular clusters with various sizes and energies, including a massive cluster of 1.6 MDa, $(CH_4)_{66396}$. To limit computer expense, only impacts on PS500 adsorbed on Au(111) were calculated. The range of kinetic energies was from 6 to 664 keV, or in terms of E/n, from ∼0.1 to 10 eV per CH_4 molecule.

Table 1 summarizes the main results concerning these simulations. First, it shows that for 45° impacts on the side of the molecule, desorption occurs for $E/n \geq 0.3$ eV. However, at 10 eV per CH_4 molecule, the PS500 polymer fragments as a result of the energetic impact. The take-off angle is around 80°, comparable to the case of Ar cluster bombardment, and with a trend of decreasing angle (more off the surface) with increasing E/n. A close examination of the data indicates that there is a perfect linear relationship between the cluster initial energy and the final kinetic energy of the desorbing molecules, reflecting similar velocities for the two centers-of-mass (Figure S-5). Figure 8 shows the case of a 20 keV $(CH_4)_{66396}$ impact, where the methane nanodrop flattens and expands radially on the gold surface, washing the PS macromolecule away with the flow of its constituent molecules. In the process, the macromolecule lifts off and its interactions with the substrate are eventually severed. It is interesting to notice that the faster CH_4 molecules on the outskirt of the expanding cluster pass at the same time below and above the PS molecule, much like a wave that would hit and carry away a still object.

The variation of the total potential energy of the PS macromolecule during the desorption event provides us with information about its degree of internal excitation (Figure 9). The cases of 20, 66, and 200 keV $(CH_4)_{66396}$ impacts (respectively, 0.3, 1, and 3 eV per CH_4 molecule), all leading

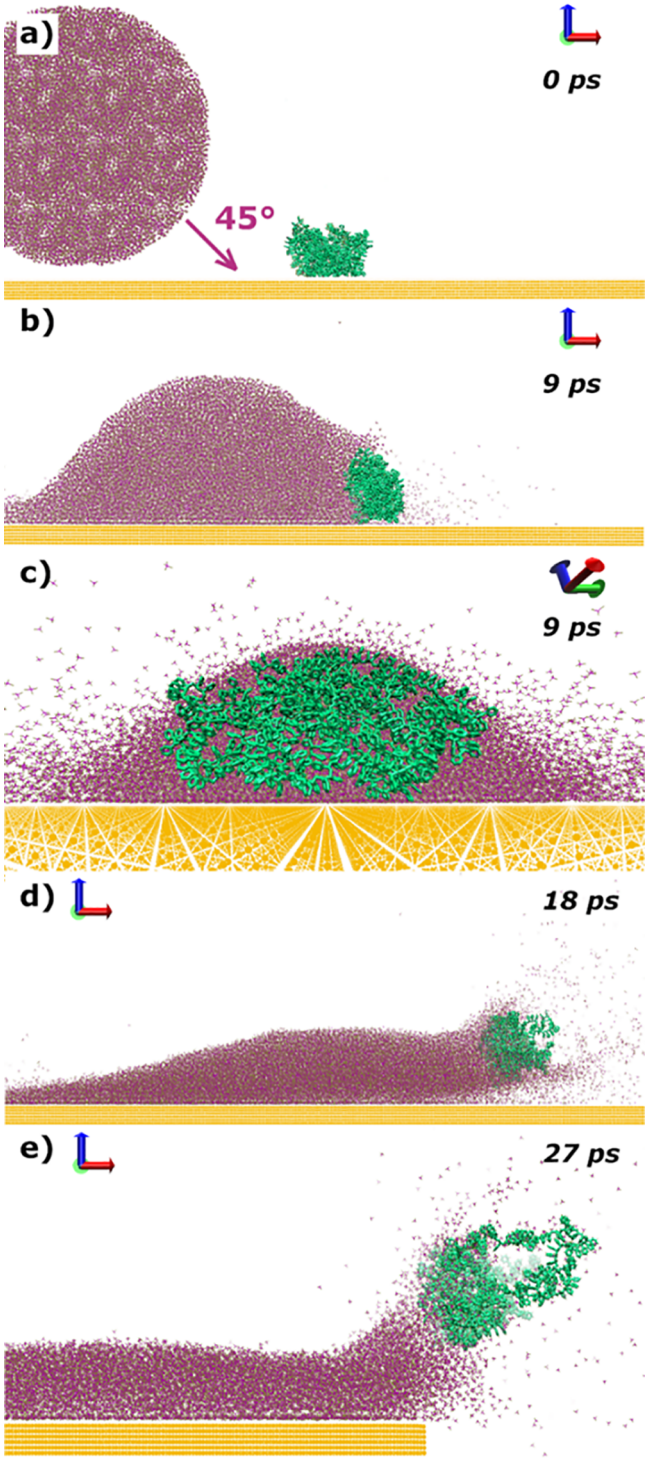

Figure 8. Time evolution of a trajectory involving sample 3 and a 20 keV $(CH_4)_{66396}$ cluster (45° incidence), impinging on the side of the PS500 molecule adsorbed on Au(111): (a) 0 ps, (b,c) 9 ps, (d) 18 ps, and (e) 27 ps. Panel (c) shows a perspective view, with a horizontal rotation of 90° clockwise with respect to the other views, as if the molecule and the Ar cluster were moving toward the reader.

to intact molecular desorption, are represented by the green, orange, and red lines, respectively. The horizontal black line indicates the potential energy of the relaxed molecule in the vacuum. The colored lines start at a lower level because of the binding to the surface prior to the impact. The time variation of the potential energy related to each individual bond vibration is

https://doi.org/10.1021/acs.jpcc.2c01196
J. Phys. Chem. C 2022, 126, 7307−7318

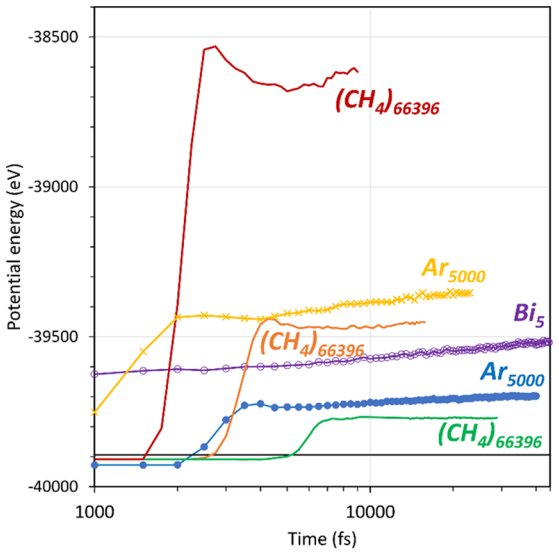

Figure 9. Time-evolution of the potential energy of the desorbing PS500 molecule for different impact scenarios. On sample 2: blue dots, 10 keV Ar_{5000} (45° incidence); violet circles, 30 keV Bi_5 (45° incidence; aiming point B in Figure 4). On sample 3: yellow crosses, 10 keV Ar_{5000}; green line, 20 keV $(CH_4)_{66396}$; orange line: 66 keV $(CH_4)_{66396}$; red line, 200 keV $(CH_4)_{66396}$.

averaged over the large number of bonds so that the total potential energy evolves smoothly with time. For the same reason, although the potential energy is only part of the total internal energy (the kinetic energy relative to the center-of-mass is not counted), they should be proportional. The final potential energy difference of the PS molecule with the reference state increases by one order of magnitude when the kinetic energy of the projectile varies from 20 to 200 keV, also suggesting linearity between the macromolecule internal energy gain and the projectile kinetic energy. At 664 keV, the internal energy is sufficient to instantly fragment the molecule.

For comparison, the potential energy curves of two different trajectories involving 10 keV Ar_{5000} bombardment are plotted on the same graph. The yellow curve corresponds to the situation of Figure 7a–c, where Ar_{5000} impinges on the PS500 molecule adsorbed on Au. It is the closest to the 66 keV $(CH_4)_{66396}$ impact curve, for which the kinetic energy per unit mass (E/amu) is comparable. Therefore, these and previous results suggest that E/n (or E/amu when comparing clusters with different chemistries) is the main parameter governing internal energy uptake by the target molecule, irrespective of, e.g., the cluster size and total energy. Two impact events on purely organic samples are also represented in Figure 9. First, the 10 keV Ar_{5000} (45°) impact (blue) transfers surprisingly little internal energy to the macromolecule in spite of its larger binding energy to the substrate. It is actually closer to the line of 20 keV $(CH_4)_{66396}$ (0.3 eV/constituent molecule). Our interpretation is that the washing mechanism, coupled with the smooth deformation of the substrate and the development of the crater rim, enables a softer emission of the macromolecule, as compared to the hard gold substrate (yellow line). In comparison, the violet line, corresponding to 30 keV Bi_5 (45°) impact B, leads to an almost twice larger increase in the molecule potential energy (and a much smaller center-of-mass velocity, see Table 1) because it lacks the correlated push of the backscattered Ar cluster atoms.

3.5. Implications for Experiments. First, our preliminary simulations with sample 1 indicate that in order to maximize sputtering upon 10 keV Ar_{5000} bombardment of a polystyrene monolayer on a polymeric substrate, incidence angles between 40 and 60° with respect to the surface normal are optimum. This justifies the use of 45° incidence in many SIMS experimental setups and also indicates that the geometry used so far in GCIB-induced molecular transfer experiments (75° incidence) should be improved for better efficiency.

MD simulations of a PS500 macromolecule desorption from a soft substrate were conducted in order to investigate and guide future molecular transfer experiments involving larger molecules than small compounds and oligomers, insulin, or even lysozyme (14 kDa). They indicate that side hits by 10 keV Ar_{5000} clusters with incidence angles >30° generally lead to such large molecule emission from the surface in spite of its mass and relatively large binding energy (56 eV). For a 45° impact trajectory, the take-off angle is 60°, the molecule velocity is ∼1 km/s, and the internal excitation of the macromolecule is relatively low—though it tends to unfold upon emission in all the tested cases. Unfolding might be less pronounced for proteins with stronger intramolecular interactions and, in particular, molecules like lysozyme, which are stabilized by a number of covalent sulfur bridges. In this respect, it should be noted that even mass spectrometry/soft landing methods reputed to be very soft, such as electrospray ionization (ESI), may lead to extended molecular conformations especially for highly charged states.[51] The molecular internal energies produced by large Ar GCIB desorption[52] are actually similar to ESI and DESI.[53] In comparison with large Ar clusters, regular time-of-flight secondary ion mass spectrometry (ToF-SIMS) analysis clusters such as 30 keV Bi_n struggle to desorb intact PS500 molecules because of fragmentation or insufficient momentum transfer from the collective motion following the impact. This is consistent with the fact that they produce secondary ions with higher average internal energies.[52]

In most molecular desorption and transfer experiments, the macro- and/or biomolecules are embedded in a film or coating, forming a complete molecular surface, at variance with our simulations where one molecule "sticks out" of the surface. Placing a fully atomistic macromolecule with the size of a protein on a soft hydrocarbon coarse-grained substrate seemed to be the best tractable approximation considering computer time issues, and it showed pronounced and interesting differences with a heavy metal substrate. Looking at both the lateral development of the crater in the organic (coarse-grained) material and the effect of the projectile atoms, either directly incident or backscattered on the PS macromolecule, it seems that similar causes should operate with similar effects in a full layer of separated, not entangled, macromolecules. The directly hit molecules should push their neighbors sideways and upwards, and they could desorb owing to the extra energy of the Ar atoms and small clusters backscattered from the crater. Experimentally, this would be impossible with polystyrene because polymer coils of that molecular weight should be entangled in a thick coating. Such a process should happen, however, with globular biomolecules such as medium-size proteins (lysozyme, horseradish peroxidase, glucose oxidase, etc.). Even if the desorption process had a lower probability of occurrence in these conditions, the fact that the crater rim would be composed entirely by such macromolecules might even increase the chances. On the other hand, there would not be more reasons for intact emission to occur from such a molecular surface than the one computed here, for normal or close to normal projectile incidence angles. Indeed, in that case, most of the impact energy

https://doi.org/10.1021/acs.jpcc.2c01196
J. Phys. Chem. C 2022, 126, 7307−7318

is lost in the depth of the sample via plastic deformation and the backscattered Ar atoms have negligible energies.

In many cases, the simulations predict intact molecule desorption within a time of tens of picoseconds. The relevant times in experiments, however, correspond to molecules, which can travel a distance of ∼1 cm in transfer configuration and ∼1 m in ToF-SIMS analysis. Assuming a typical center-of-mass velocity of 1 km/s, as computed for 10 keV Ar_{5000} impacts on PS500, the time to the collector or to the detector should be from μs to ms (taking into account the fact that, in the second case, the ions are usually accelerated by keV voltages after emission). Such times are out of reach of MD simulations and could lead to extensive unimolecular dissociation of the most excited molecules. Therefore, in comparison with experiments, the MD predictions of this article are rather optimistic. However, the experimental proof that various molecules, including 14 kDa lysozymes, could be transferred without damage by the same clusters shows that it is possible for sizeable molecules. The internal energy transferred to the molecules should be proportional to their size, but the unimolecular dissociation theories indicate that the probability of a molecule to sustain a certain amount of internal energy for a given time without dissociating is also proportional to its size, so that larger molecules should also have a good probability to survive.[54] For this reason, the desorption step seems to be the most critical in transfer experiments and, additionally, the ionization step in mass spectrometry. To our knowledge, there are few measurements decoupling ionization from desorption, but there exist some indications that ionization probability decreases faster than desorption efficiency with an increasing Ar cluster size.[55]

Desorption of large molecules from a noble metal substrate, not applicable for transfer experiments, could be an interesting avenue for large molecule analysis since the MD simulations predict easier desorption than from soft substrates. However, this is also conditioned to the ionization efficiency and cationizing agents might be needed. In addition, the calculated internal energies of the PS500 macromolecules are generally higher when they are desorbed from gold than from PE, so that a different tuning of the cluster projectile size or energy might be needed for optimal results. For that purpose, the use of larger projectiles, such as our massive methane cluster, or smaller impact energies might be more effective.

4. CONCLUSIONS

The MD simulations of projectile−surface interactions show that 10 keV Ar_{5000} clusters are able to desorb a PS macromolecule of 60 kDa from both polymeric and metallic substrates. In doing so, they indicate that the mass range of the molecules transferred in the gas phase by cluster ions should not be limited to the largest molecule measured so far (14 kDa in molecular transfer experiments[6] and, for instance, in electrospray-droplet impact MS[56]). They also predict a range of incidence angles and energies leading to intact molecular emission. In all cases of large cluster impacts, the take-off angle of the macromolecule is larger than the incidence of the projectile. Bombardment by a massive methane projectile (6.6×10^4 units) does not induce qualitatively different results, and in general, the energy per atom or energy per unit mass remains the deciding factor concerning the survival or dissociation of the bombarded molecule. The potential energy uptakes of the PS macromolecule absorbed on gold when bombarded by 10 keV Ar_{5000} or by 66 keV $(CH_4)_{66396}$ are comparable. For identical bombardment conditions (10 keV Ar_{5000} at 45° incidence), the potential energy and the translational energy uptakes are, respectively, 3 and 4 times larger for the gold substrate than for the polymeric substrate. In contrast with large Ar clusters, Bi_5 projectiles largely fail at desorbing the intact PS500 molecule for 16 of the 17 tested impact points on the surface for two identified reasons. First, when the impact is close to the molecule, it often gets damaged by a recoil atom generated in the collision cascade. Second, for close impacts that do not immediately fragment the molecule, the momentum transferred by the collective dynamics of the crater expansion remains insufficient for molecular lift off. The mechanistic analysis of the trajectories indicates that, in addition, 10 keV Ar_{5000} projectiles with 45−75° incidence directly transfer momentum to the macromolecule via their backscattered Ar atoms and small clusters. Consequently, the macromolecule leaves the surface with a center-of-mass velocity equal to or larger than 1 km/s.

■ ASSOCIATED CONTENT

Supporting Information

The Supporting Information is available free of charge at https://pubs.acs.org/doi/10.1021/acs.jpcc.2c01196.

Five supplementary figures: (Figure S-1) experiment of molecular transfer of PS oligomers from a solid target to a collector, (Figures S-2 and S-3) snapshots showing details of the molecular dynamics, (Figure S-4) top view of sample 3, and (Figure S-5) graph of the desorbed PS500 molecule velocity as a function of the projectile velocity (PDF)

■ AUTHOR INFORMATION

Corresponding Author

Arnaud Delcorte − *Institute of Condensed Matter and Nanoscience, Université catholique de Louvain, 1348 Louvain-la-Neuve, Belgium;* orcid.org/0000-0003-4127-8650; Email: Arnaud.delcorte@uclouvain.be

Complete contact information is available at: https://pubs.acs.org/10.1021/acs.jpcc.2c01196

Notes

The author declares no competing financial interest.

■ ACKNOWLEDGMENTS

Professor B. J. Garrison is gratefully acknowledged for granting us access to her MD simulation code. A.D. is a Research Director of the Belgian Fonds National pour la Recherche Scientifique (FNRS). This research was supported by the Federation Wallonie Bruxelles, through the project "iBEAM" funded by its research program "Actions de Recherche Concertees" (grant no. 18/23-090) and by the grant FNRS-PDR T.0052.22. Computational resources were provided by the Institut de Calcul Intensif et de Stockage de Masse (CISM) at Université Catholique de Louvain. The theoretical and computational biophysics group of the University of Illinois at Urbana−Champaign is acknowledged for the development and free access to the VMD software (Humphrey, W.; Dalke, A.; Schulten, K. VMD−Visual Molecular Dynamics. *J. Mol. Graphics* 1996, **14**, 33−38).

■ REFERENCES

(1) Norde, W. Adsorption of Proteins at Solid-Liquid Interfaces. *Cells Mater.* **1995**, *5*, 9.

(2) Lundqvist, M.; Sethson, I.; Jonsson, B.-H. Protein Adsorption onto Silica Nanoparticles: Conformational Changes Depend on the Particles' Curvature and the Protein Stability. *Langmuir* **2004**, *20*, 10639−10647.
(3) Norde, W.; Horbett, T. A.; Brash, J. L. Proteins at Interfaces III: Introductory Overview. *ACS Symp. Ser.* **2012**, *1120*, 1−34.
(4) Johnson, G. E.; Gunaratne, D.; Laskin, J. Soft- and Reactive Landing of Ions Onto Surfaces: Concepts and Applications. *Mass Spectrom. Rev.* **2016**, *35*, 439−479.
(5) Yin, L.; Zhang, Z.; Liu, Y.; Gao, Y.; Gu, J. Recent advances in single-cell analysis by mass spectrometry. *Analyst* **2019**, *144*, 824−845.
(6) Delmez, V.; Degand, H.; Poleunis, C.; Moshkunov, K.; Chundak, M.; Dupont-Gillain, C.; Delcorte, A. Deposition of Intact and Active Proteins In Vacuo Using Large Argon Cluster Ion Beams. *J. Phys. Chem. Lett.* **2021**, *12*, 952−957.
(7) Lorenz, M.; Zhang, J.; Shard, A. G.; Vorng, J.-L.; Rakowska, P. D.; Gilmore, I. S. Method for Molecular Layer Deposition Using Gas Cluster Ion Beam Sputtering with Example Application In Situ Matrix-Enhanced Secondary Ion Mass Spectrometry. *Anal. Chem.* **2021**, *93*, 3436−3444.
(8) Moshkunov, K.; Tomasetti, B.; Daphnis, T.; Delmez, V.; Vanvarenberg, K.; Préat, V.; Lorenz, M.; Quanico, J.; Baggerman, G.; Lemiere, F.; et al. Improvement of biomolecular analysis in thin films using in situ matrix enhanced secondary ion mass spectrometry. *Analyst* **2021**, *146*, 6506−6519.
(9) Lorenz, M.; Shard, A. G.; Counsell, J. D. P.; Hutton, S.; Gilmore, I. S. Angular Distribution of Molecules Sputtered by Gas Cluster Ion Beams and Implications for Secondary Neutral Mass Spectrometry. *J. Phys. Chem. C* **2016**, *120*, 25317−25327.
(10) Delcorte, A.; Delmez, V.; Dupont-Gillain, C.; Lauzin, C.; Jefford, H.; Chundak, M.; Poleunis, C.; Moshkunov, K. Large Cluster Ions: Soft Local Probes and Tools for Organic and Bio Surfaces. *Phys. Chem. Chem. Phys.* **2020**, *22*, 17427−17447.
(11) Delmez, V.; Tomasetti, B.; Daphnis, Th.; Poleunis, C.; Lauzin, C.; Dupont-Gillain, Ch.; Delcorte, A. Gas cluster ion beam as a versatile soft-landing tool for the controlled construction of thin (bio)films, *ACS Appl. Biomaterials*, 2022, submitted.
(12) Schneider, P.; Verloh, F.; Portz, A.; Aoyagi, S.; Rohnke, M.; Dürr, M. Direct Analysis of Ion-Induced Peptide Fragmentation in Secondary-Ion Mass Spectrometry. *Anal. Chem.* **2020**, *92*, 15604−15610.
(13) Lockyer, N. P. In *Methods in Molecular Biology − Electron Microscopy: Methods and Protocols*; Kuo, J., Ed.; Springer Science +Business Media: New York, 2014; Vol. *1117*, pp. 707−732.
(14) Passarelli, M. K.; Pirkl, A.; Moellers, R.; Grinfeld, D.; Kollmer, F.; Havelund, R.; Newman, C. F.; Marshall, P. S.; Arlinghaus, H.; Alexander, M. R.; et al. The 3D OrbiSIMS: Label-Free Metabolic Imaging with Subcellular Lateral Resolution and High Mass-Resolving Power. *Nat. Methods* **2017**, *14*, 1175−1183.
(15) Kotowska, A. M.; Trindade, G. F.; Mendes, P. M.; Williams, P. M.; Aylott, J. W.; Shard, A. G.; Alexander, M. R.; Scurr, D. J. Protein identification by 3D OrbiSIMS to facilitate in situ imaging and depth profiling. *Nat. Commun.* **2020**, *11*, 5832.
(16) Dimovska Nilsson, K.; Karagianni, A.; Kaya, I.; Henricsson, M.; Fletcher, J. S. (CO2)n+, (H2O)n+, and (H2O)n+ (CO2) gas cluster ion beam secondary ion mass spectrometry: analysis of lipid extracts, cells, and Alzheimer's model mouse brain tissue. *Anal. Bioanal. Chem.* **2021**, *413*, 4181−4194.
(17) Sämfors, S.; Fletcher, J. S. Lipid Diversity in Cells and Tissue Using Imaging SIMS. *Annu. Rev. Anal. Chem.* **2020**, *13*, 249−271.
(18) Garrison, B. J.; Delcorte, A.; Krantzman, K. D. Molecule liftoff from surfaces. *Acc. Chem. Res.* **2000**, *33*, 69−77.
(19) Harrison, D. E., Jr.; Kelly, P. W.; Garrison, B. J.; Winograd, N. Low energy ion impact phenomena on single crystal surfaces. *Surf. Sci.* **1978**, *76*, 311−322.
(20) Garrison, B. J. Organic molecule ejection from surfaces due to heavy particle bombardment. *J. Am. Chem. Soc.* **1982**, *104*, 6211−6217.
(21) Garrison, B. J.; Postawa, Z. Computational View of Surface Based Organic Mass Spectrometry. *Mass Spectrom. Rev.* **2008**, *27*, 289−315.
(22) Rzeznik, L.; Czerwinski, B.; Garrison, B. J.; Winograd, N.; Postawa, Z. Microscopic Insight into the Sputtering of Thin Polystyrene Films on Ag{111} Induced by Large and Slow Ar Clusters. *J. Phys. Chem. C* **2008**, *112*, 521−531.
(23) Delcorte, A.; Garrison, B. J.; Hamraoui, K. Dynamics of Molecular Impacts on Soft Materials: From Fullerenes to Organic Nanodrops. *Anal. Chem.* **2009**, *81*, 6676−6686.
(24) Aoki, T. Molecular dynamics simulations of cluster impacts on solid targets: implantation, surface modification, and sputtering. *J. Comput. Electron.* **2014**, *13*, 108−121.
(25) Samela, J.; Nordlund, K. Atomistic Simulation of the Transition from Atomistic to Macroscopic Cratering. *Phys. Rev. Lett.* **2008**, *101*, No. 027601.
(26) Schneider, P.; Dürr, M. Cluster-induced desorption investigated by means of molecular dynamics simulations—Microsolvation in clusters of polar and nonpolar constituents. *J. Chem. Phys.* **2019**, *150*, 214301.
(27) Delcorte, A.; Debongnie, M. Macromolecular Sample Sputtering by Large Ar and CH4 Clusters: Elucidating Chain Size and Projectile Effects with Molecular Dynamics. *J. Phys. Chem. C* **2015**, *119*, 25868−25879.
(28) Mücksch, C.; Anders, C.; Gnaser, H.; Urbassek, H. M. Dynamics of L-Phenylalanine Sputtering by Argon Cluster Bombardment. *J. Phys. Chem. C* **2014**, *118*, 7962−7970.
(29) Delcorte, A.; Cristaudo, V.; Lebec, V.; Czerwinski, B. Sputtering of polymers by keV clusters: Microscopic views of the molecular dynamics. *Int. J. Mass Spectrom.* **2014**, *370*, 29−38.
(30) Czerwinski, B.; Rzeznik, L.; Paruch, R.; Garrison, B. J.; Postawa, Z. Effect of impact angle and projectile size on sputtering efficiency of solid benzene investigated by molecular dynamics simulations. *Nucl. Instrum. Methods Phys. Res., Sect. B* **2011**, *269*, 1578−1581.
(31) Pratihar, S.; Kohale, S. C.; Bhakta, D. G.; Laskin, J.; Hase, W. L. Dynamics of energy transfer and soft-landing in collisions of protonated dialanine with perfluorinated self-assembled monolayer surfaces. *Phys. Chem. Chem. Phys.* **2014**, *16*, 23769−23778.
(32) Somer, A. M.; Macaluso, V.; Barnes, G. L.; Yang, L.; Pratihar, S.; Song, K.; Hase, W. L.; Spezia, R. Role of Chemical Dynamics Simulations in Mass Spectrometry Studies of Collision-Induced Dissociation and Collisions of Biological Ions with Organic Surfaces. *J. Am. Soc. Mass Spectrom.* **2020**, *31*, 2−24.
(33) Smiley, E. J.; Postawa, Z.; Wojciechowski, I. A.; Winograd, N.; Garrison, B. J. Coarse-grained molecular dynamics studies of cluster-bombarded benzene crystals. *Appl. Surf. Sci.* **2006**, *252*, 6436−6439.
(34) Delcorte, A.; Garrison, B. J. Sputtering Polymers with Buckminsterfullerene Projectiles: A Coarse-Grain Molecular Dynamics Study. *J. Phys. Chem. C* **2007**, *111*, 15312−15324.
(35) Hamraoui, K.; Delcorte, A. Effects of molecular orientation and size in sputtering of model organic crystals. *J. Phys. Chem. C* **2010**, *114*, 5458−5467.
(36) Stuart, S. J.; Tutein, A. B.; Harrison, J. A. A reactive potential for hydrocarbons with intermolecular interactions. *J. Chem. Phys.* **2000**, *112*, 6472−6486.
(37) Postawa, Z.; Czerwinski, B.; Szewczyk, M.; Smiley, E. J.; Winograd, N.; Garrison, B. J. Enhancement of Sputtering Yields Due to C60 versus Ga Bombardment of Ag{111} As Explored by Molecular Dynamics Simulations. *Anal. Chem.* **2003**, *75*, 4402−4407.
(38) Stave, M. S.; Sanders, D. E.; Raeker, T. J.; DePristo, A. E. Corrected effective medium method. V. Simplifications for molecular dynamics and Monte Carlo simulations. *J. Chem. Phys.* **1990**, *93*, 4413−4426.
(39) Liu, K. S. S.; Yong, C. W.; Garrison, B. J.; Vickerman, J. C. Molecular Dynamics Simulations of Particle Bombardment Induced Desorption Processes: Alkanethiolates on Au(111). *J. Phys. Chem. B* **1999**, *103*, 3195−3205.
(40) Delcorte, A.; Garrison, B. J. Water nanodroplet impacts on surfaces: Effect of the substrate nature. *Nucl. Instrum. Methods Phys. Res., Sect. B* **2013**, *303*, 179−183.

https://doi.org/10.1021/acs.jpcc.2c01196
J. Phys. Chem. C 2022, 126, 7307−7318

(41) Tomsic, A.; Schröder, H.; Kompa, K.-L.; Gebhardt, C. R. Impact dynamics of molecular clusters on surfaces: Fragmentation patterns and anisotropic effects. *J. Chem. Phys.* **2003**, *119*, 6314−6323.
(42) Sun, S. N.; Urbassek, H. M. Role of cohesive energy in droplet fragmentation. *Phys. Rev. B* **2011**, *84*, No. 056315.
(43) O'connor, D. J.; Biersack, J. P. Comparison of theoretical and empirical interatomic potentials. *Nucl. Instrum. Methods Phys. Res., Sect. B* **1986**, *15*, 14−19.
(44) Delcorte, A.; Leblanc, C.; Poleunis, C.; Hamraoui, K. Computer Simulations of the Sputtering of Metallic, Organic, and Metal−Organic Surfaces with Bin and C60 Projectiles. *J. Phys. Chem. C* **2013**, *117*, 2740−2752.
(45) Yuan, H. K.; Chen, H.; Kuang, A. L.; Miao, Y.; Xiong, Z. H. Density-functional study of small neutral and cationic bismuth clusters Bi(n) and Bi(n) (+)(n=2-24). *J. Chem. Phys.* **2008**, *128*, No. 094305.
(46) Delcorte, A.; Wojciechowski, I.; Gonze, X.; Garrison, B. J.; Bertrand, P. Single and double cationization of organic molecules in SIMS. *Int. J. Mass Spectrom.* **2002**, *214*, 213−232.
(47) Seah, M. P.; Spencer, S. J.; Shard, A. G. Angle Dependence of Argon Gas Cluster Sputtering Yields for Organic Materials. *J. Phys. Chem. B* **2015**, *119*, 3297−3303.
(48) Delcorte, A.; Garrison, B. J. Desorption of large molecules with light-element clusters: Effects of cluster size and substrate nature. *Nucl. Instrum. Methods Phys. Res., Sect. B* **2011**, *269*, 1572−1577.
(49) Moritani, K.; Kanai, M.; Goto, K.; Ihara, I.; Inui, N.; Mochiji, K. Secondary ion emission from insulin film bombarded with methane and noble gas cluster ion beams. *Nucl. Instrum. Methods Phys. Res., Sect. B* **2013**, *315*, 300−303.
(50) Wucher, A.; Tian, H.; Winograd, N. A mixed cluster ion beam to enhance the ionization efficiency in molecular secondary ion mass spectrometry. *Rapid Commun. Mass Spectrom.* **2014**, *28*, 396−400.
(51) Metwally, H.; Duez, Q.; Konermann, L. Chain Ejection Model for Electrospray Ionization of Unfolded Proteins: Evidence from Atomistic Simulations and Ion Mobility Spectrometry. *Anal. Chem.* **2018**, *90*, 10069−10077.
(52) Fu, T.; Della-Negra, S.; Touboul, D.; Brunelle, A. Internal Energy Distribution of Secondary Ions Under Argon and Bismuth Cluster Bombardments: "Soft" Versus "Hard" Desorption−Ionization Process. *J. Am. Soc. Mass Spectrom.* **2019**, *30*, 321−328.
(53) Nefliu, M.; Smith, J. N.; Venter, A.; Cooks, R. G. Internal Energy Distributions in Desorption Electrospray Ionization (DESI). *J. Am. Soc. Mass Spectrom.* **2008**, *19*, 420−427.
(54) Robinson, P. J.; Holbrook, K. A. *Unimolecular reactions*; Wiley: New York, 1972.
(55) Rabbani, S.; Barber, A. M.; Fletcher, J. S.; Lockyer, N. P.; Vickerman, J. C. TOF-SIMS with Argon Gas Cluster Ion Beams: A Comparison with C60+. *Anal. Chem.* **2011**, *83*, 3793−3800.
(56) Hiraoka, K.; Mori, K.; Asakawa, D. Fundamental aspects of electrospray droplet impact/SIMS. *J. Mass Spectrom.* **2006**, *41*, 894−902.

https://doi.org/10.1021/acs.jpcc.2c01196
J. Phys. Chem. C 2022, 126, 7307−7318